Pacific Northwest
NATIONAL LABORATORY

PNNL-30228

Computational Tool for Cosmic Ray Flux and Cosmogenic Activation Production Rate

August 2020

Mendez, Nicholas

U.S. DEPARTMENT OF ENERGY

Prepared for the U.S. Department of Energy
under Contract DE-AC05-76RL01830

DISCLAIMER

PACIFIC NORTHWEST NATIONAL LABORATORY
operated by
BATTELLE
for the
UNITED STATES DEPARTMENT OF ENERGY
under Contract DE-AC05-76RL01830

Printed in the United States of America

Available to DOE and DOE contractors from
the Office of Scientific and Technical Information,
P.O. Box 62, Oak Ridge, TN 37831-0062
www.osti.gov
ph: (865) 576-8401
fox: (865) 576-5728
email: reports@osti.gov

Available to the public from the National Technical Information Service
5301 Shawnee Rd., Alexandria, VA 22312
ph: (800) 553-NTIS (6847)
or (703) 605-6000
email: info@ntis.gov
Online ordering: http://www.ntis.gov

PNNL-30228

Computational Tool for Cosmic Ray Flux and Cosmogenic Activation Production Rate

August 2020

Mendez, Nicholas

Prepared for
the U.S. Department of Energy
under Contract DE-AC05-76RL01830

Pacific Northwest National Laboratory
Richland, Washington 99354

Computational Tool for Cosmic Ray Flux and Cosmogenic Activation Production Rate

Nicholas Mendez

Silicon charge couple devices (CCDs) are used in direct detection dark matter searches. Silicon can be obtained with very high purity and negligible amounts of radioactive contaminants. However, silicon exposed to cosmic rays can be activated, leading to the buildup of radioactive isotopes such as tritium. The decay of tritium can produce signals that cannot be distinguished from the expected signals of dark matter interactions and tritium produced by cosmic rays is expected as one of the leading sources of background for next-generation experiments. The cosmic ray flux depends on variables such as geomagnetic latitude and longitude, atmospheric depth/altitude, solar activity, and surrounding environment for example. The goal of this work is to create a tool that will evaluate the total cosmic ray exposure and related tritium production rate for any given exposure history of a silicon detector. EXcel-based Program for calculation Atmospheric Cosmic-ray Spectrum (EXPACS) was used to obtain the cosmic ray fluxes. We have worked on creating a 3-dimensional gird that spans latitude, longitude, and altitude, and can be used to interpolate the cosmic ray flux at any given location. This computation tool additionally has use for work requiring knowledge of the cosmic ray flux at multiple locations.

I. INTRODUCTION

A. Dark Matter Search

Some of the earliest evidence for the existence of dark matter exists from studying the rotational velocities of galaxies [1]. Other evidence for dark mater includes gravitational lensing and galaxy cluster collisions [2]. Previous searches for dark matter, such as XENON at Gran Sasso National Laboratory, have focused on the search the Weakly Interacting Massive Particles (WIMPs) with a mass in the 100 GeV range [1]. Next generation experiments, such as OSCURA, are looking for dark matter particles with mass in the sub-GeV range using CCD's [3].

B. CCD Physics

CCD's are used in dark matter searches for their ability to make detections on the scale of single electrons [4]. Silicon CCD's work by collecting unbounded electrons from a silicon atom. The CCD is split into pixels that contain the electrons by creating an electric potential within the pixel to store the charges. Each charge within the pixels is shifted through the CCD to a readout where the charges in each pixel are used to record the energy within each pixel.

To detect dark matter, a dark matter particle can come and knock off an electron from the silicon atom which ionizes nearby silicon atoms. These free electrons are gathered at the pixel and moved through the CCD for the signal to be readout and recorded [5]. A pictorial representation is shown in Figure 1.

C. Cosmic Rays & Cosmogenic Activation

The primary source of cosmic rays come from space with most particles being protons (92%) followed by alpha particles (6%) and heavier atomic nuclei (2%) [6]. As these particles

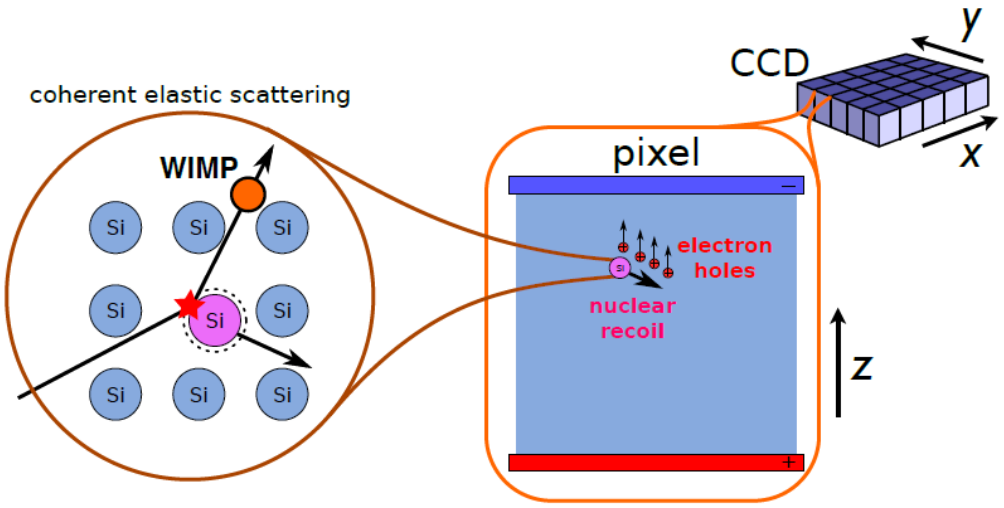

FIG. 1. A visual representation of dark matter detection within a silicon CCD from the DAMIC-M experiment [5]. The diagram shows a WIMP interacting with the silicon nucleus though a dark matter particle can also knock off a bound electron.

interact with the earth's atmosphere, a cascade of particles are created from these interactions (neutrons, photons, muons, electrons, pions, and heavier atomic nuclei). Charged particles interact with the earth's magnetic field impacting cascade showers. A schematic is shown in Figure 2. Cosmic ray interactions with matter is of interest for detectors such as silicon CCD's. The interaction of cosmic rays with atomic nuclei can produce radioactive isotopes which can impact the detector sensitivity and is known as cosmogenic activation [7]. For silicon CCD's, the production of tritium can be especially concerning in the search for dark matter.

D. Tritium

Tritium is a pure beta emitter with a half-life of 12.32 years [8] and these betas can ionize neighboring atoms within the CCD. These ionized atoms create electron hole pairs which are detected in the CCD and recorded as a detection event. The signals produced by the decay of tritium cannot be distinguished from the expected signal for a dark matter detection. It is therefore desirable to shield the silicon used to produce the CCD during the time that is spent above ground before the detector is installed deep underground.

II. BACKGROUND RESEARCH

A. Production Rates

The nuclear production rates depend on three factors: particle flux, reaction cross section, and number density of the nuclei of interest. Production rates can be calculated using Eq 1.

$$\int_{E_2}^{E_1} \phi(E) * \sigma(E) * n \; dE \tag{1}$$

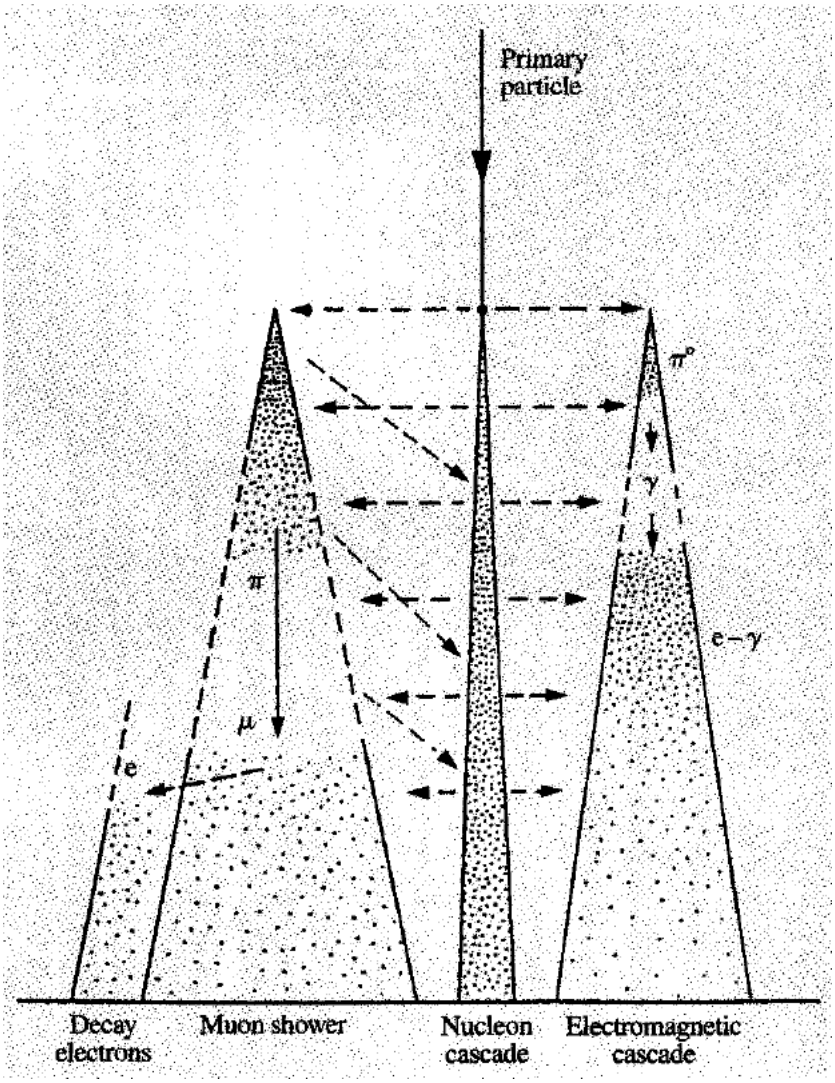

FIG. 2. A visual representation of particle showers as particle interacts with the earth's atmosphere as shown in Ziegler [6].

The particle flux, ϕ(E), has units of (particles/cm^2/s/MeV), the neutron-induced tritium production cross section, σ(E) , has units of (cm^2), and the number density, n, has units of (atoms/kg). The number density is calculated to be 2.144E+25 atoms/kg for silicon.

This project utilizes a model from the INCL++ (ALBA 07) nuclear code for the silicon cross section [9] in all production rate calculations and is shown in Figure 3. The energy range of the plotted cross section data is 11 MeV – 5 GeV, though the cross section continues past 5 GeV (the neutron flux past 5 MeV is minimal.)

B. Particle Fluxes

Our primary interest lies with neutrons, protons, muons, and photons, with photons being a major portion of the cosmic ray flux (percentage varies by location) . Factors impacting the cosmic ray flux that is included in this work are geomagnetic latitude and longitude, altitude, solar cycle, and environmental factors (such as a being located on the ground or

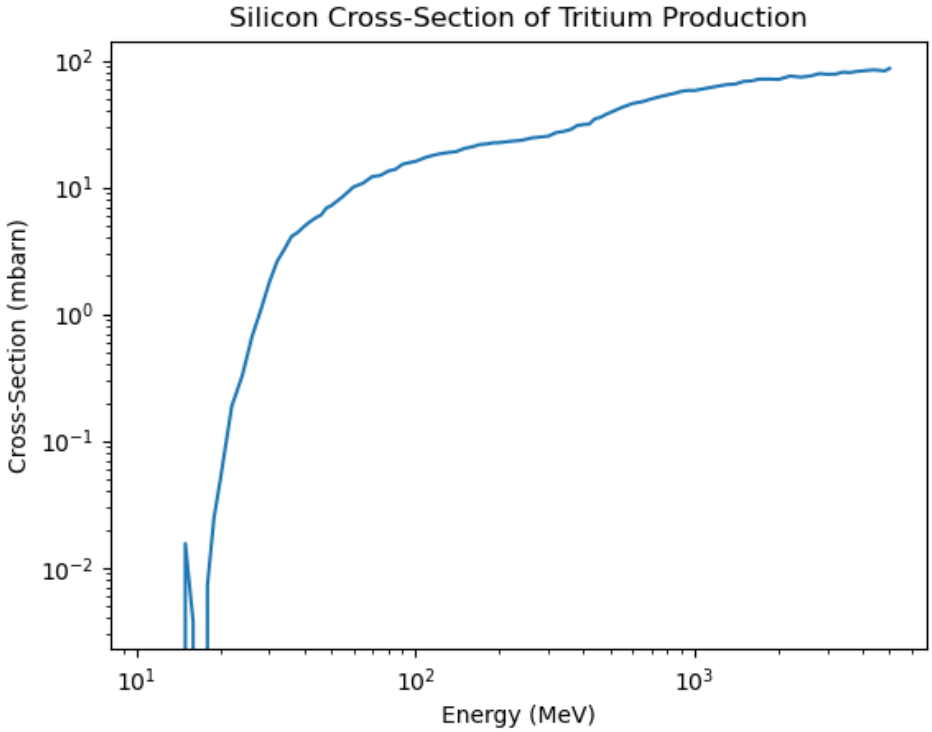

FIG. 3. Silicon cross section from the INCL++ (ALBA 07) code.

airplane).

EXPACS [10–13] is a computational tool that can calculate the cosmic ray flux of neutrons, muons, photons, electrons, protons, positrons, and charged particles with a charge up to nickel (Z=29). EXPACS is developed using the Particle and Heavy Ion Transport code System (PHITS) using a series of Monte-Carlo simulations to create a model for the particles fluxes that have been compared to experimental measurements [10 and 11]. The model for EXPACS was created using 28 concentric shells to resemble various altitudes, up to 20km (20 g/cm^2) for the earth using data from US Standard Atmosphere 1976 [12 and 13].

EXPACS has a simple input interface that accepts height in the format of either distance (km or ft), pressure (hPa), atmospheric depth (g/cm^2), or the Mass-Spectrometer-Incoherent-Scatter (MSIS) altitude (km). Users can also input the geographic latitude and longitude (degrees) or the geomagnetic cutoff rigidity (GV). Dates can be varied to get a particle flux with the latest date as of submission of this report being May 25, 2020. The surrounding environment can be varied between ideal atmosphere, ground (water fraction ranging from 0 to 1), cabin-location (mass in unit of 100ton), or pilot-location to simulate an aircraft (mass in unit of 100ton). The neutron flux energy range is from 0.01 eV to 897 GeV while the energy range for all other particles is 0.01 MeV to 897 GeV

One of the most referenced neutron particle flux spectrum, the “Gordon Spectrum” [14], shows the neutron spectrum of New York City at sea-level. Before deciding to use EXPACS for our work, we compared the EXPACS spectrum to the Gordon Spectrum using the same location and environmental inputs used for the Gordon Spectrum. The measurement for the Gordon Spectrum occurred at Yorktown Heights, NY (elevation corrected to sea level). The measurements made by Gordon lasted from September 2002 to June 2003 so the date of February 15, 2003 was chosen as the midpoint within the measurement dates. All EXPACS inputs are recorded in Table I and the comparison of the Gordon Spectrum to the

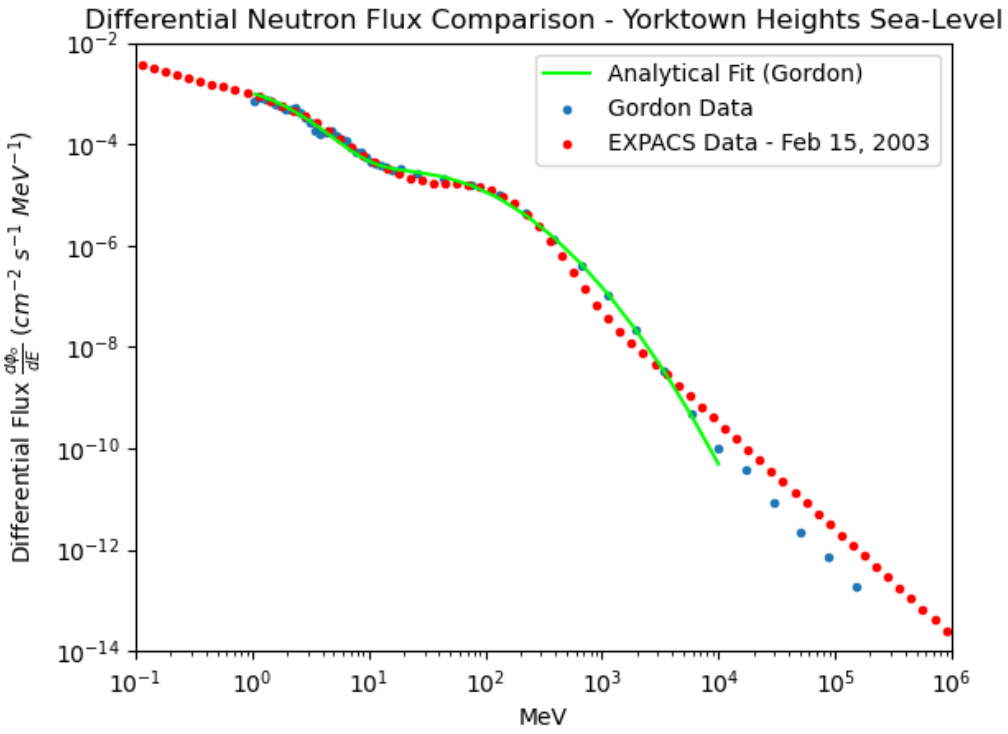

FIG. 4. At low energies, the Gordon Spectrum, Gordon Analytical Fit, and EXPACS spectrum are comparable. As the energies of the neutrons increase, the Gordon and EXPACS data begin to diverge. The fitted equation is valid in the energy range of 0.1MeV to 10GeV [14].

TABLE I. The imputed EXPACS conditions for each of the explored locations for the discussed plots.

Figure	Latitude (degrees)	Longitude (degrees)	Altitude/ Atmospheric Depth	Date	Surrounding Environment	Local Effect Parameter
Gordon	41.277	-73.781	0 ft	Feb 15, 2003	Ground	0.2
Altitude	-44.00	-118.17	Varies	July 1, 1956	Cabin	0.03
Latitude	Varies	-20.0	1033 g/cm^2	Jan 1, 1955	Ground	1
Longitude	-25,40,0	Varies	1033 g/cm^2	Jan 1, 1955	Ground	1,0
Solar Cycle	39.35	-106.43	3.621 km	Varies	Ground	0.2

EXPACS replication is shown in Figure 4. Using the Gordon Analytical Fit, the calculated neutron flux is 306 neutrons/kg/day while the EXPACS calculated neutron spectrum is 279 neutrons/kg/day with a percent difference of 9.23% which is within the experimental uncertainty of the Gordon neutron flux measurements, which are estimated to be between 10-15% above 10 MeV [14]. The neutron flux was calculated by integrating the differential neutron flux spectrum over the energy range of 10 MeV – 10 GeV.

Given the variation of the earth's magnetic field, it is desirable to understand how the particle flux varies positionally over the earth. Measurements of neutron flux over altitude are shown in Figure 5. The same trend is observed in the EXPACS recreation of the Hess plot. At higher altitudes (smaller atmospheric depth values) the neutron flux will be at its maximum due to a smaller air density, and subsequently less particle interactions, while at

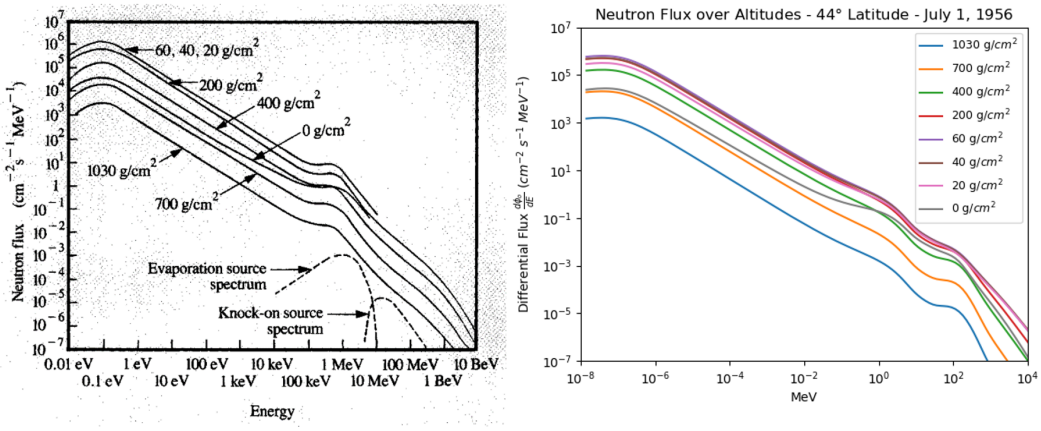

FIG. 5. Left-Plot of neutron flux over altitude as a function of atmospheric depth [6]. Right-EXPACS reproduction of the previous experimental measurement as a function of atmospheric depth.

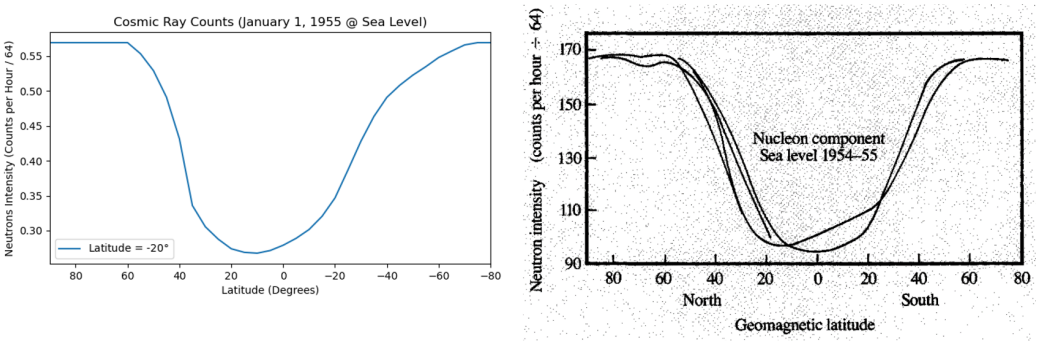

FIG. 6. Left - The variation in neutron flux intensity over latitude created from EXPACS data. Right - Measurements of the neutron intensity done in Ref [16] and plotted in Ziegler [6].

lower altitudes (higher atmospheric depth values) the possibilities of particle interactions is much higher. The Hess plot was created at Crooked Creek Laboratory on White Mountain, CA and with flyovers over the continental United States during the summer of 1956 [15]. The neutron spectrum was corrected to a latitude of 44 degrees. Measurements by Hess were made in a trailer so we assumed cabin-location of 0.03 Mass (100ton) based off typical trailer weights that could house the detectors [15].

Previous work has been done to plot the variation of neutron flux over latitude [6 and 16]. Figure 6 shows the neutron intensity (defined as counts per hour divided by 64) over latitude. Figure 6 is produced by taking the neutron energy spectrum and integrating over all energies (0.01 eV – 897 MeV) to get flux values with units of (particles/cm^2/s).

The experimental measurements were made by placing a detector on a boat and moving from one of earth's poles to the other to collect data [16]. It is not known what route or what energy the detector used was measuring [6] so a longitude of -20°was chosen as the most direct path in the Atlantic Ocean to each pole. When comparing the highest neutron intensity to the lowest, there is nearly a factor of 2 difference which is also evident in the EXPACS reproduction.

For plotting the neutron flux over longitude, the neutron flux was calculated by obtaining the neutron energy spectrum for each location and integrating the spectrum over the energy range (0.01 eV – 897 MeV). The results are shown in Figure 7. The greatest change in geomagnetic cutoff rigidity (the energy needed for a charged particle to reach the ground)

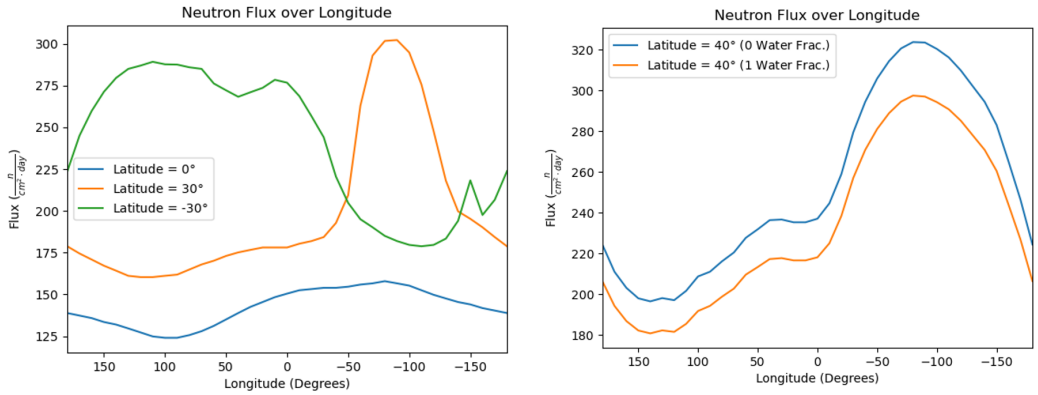

FIG. 7. Left - Changes in neutron flux over different longitudes using data from EXPACS. Right - The change in neutron flux by varying the water fraction from 0 to 1. Longitude range -180°to 180°

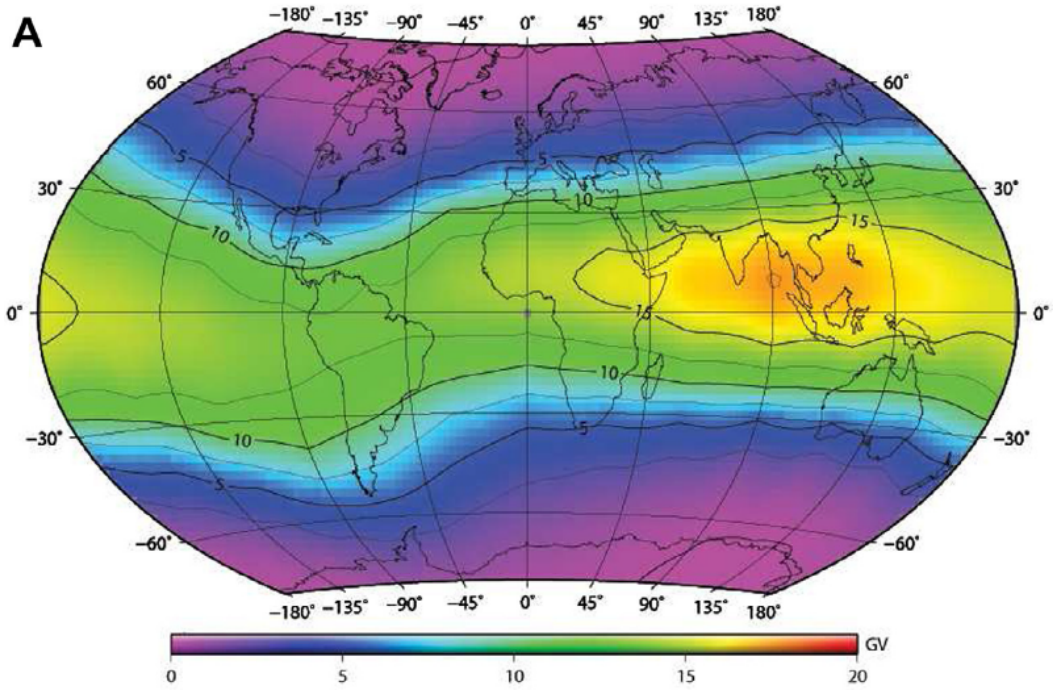

FIG. 8. Vertical geomagnetic rigidity cutoffs over the Earth from Ref [17].

occurs at around ±30°latitude [17], a global vertical geomagnetic cutoff rigidity is shown in Figure 8, and were chosen in hopes of observing significant chances in neutron flux over longitude. There is significant change in the longitude at ±30 degrees latitude and minimal change near the equator.

The cosmic ray flux also depends on the solar cycle and detailed measurement of the intensity has been measured and recorded since 1951 [6]. A detector was placed outside the Homestake Mine in Colorado and the relative intensity is plotted as a percent change from the 1954 flux. A comparison between the measured data and the EXPACS recreation is shown in Figure 9. The sampled rate for EXPACS was taken every 6 months starting on April 1, 1951. The same sinusoidal shape is observed in the EXPACS recreation though the relative intensity is about 5% higher for years 1957-1960 and 1990 than what has been

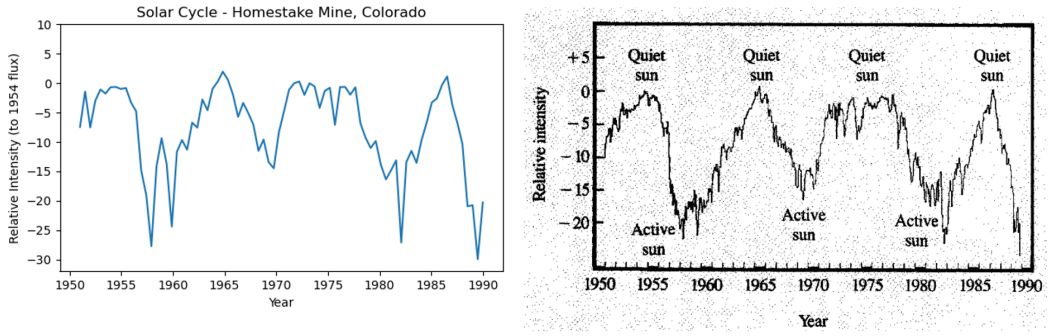

FIG. 9. Left-Relative flux to 1954 with water fraction=0.2 using EXPACS data. Right-Measurements made at Homestake Mine in Colorado [6].

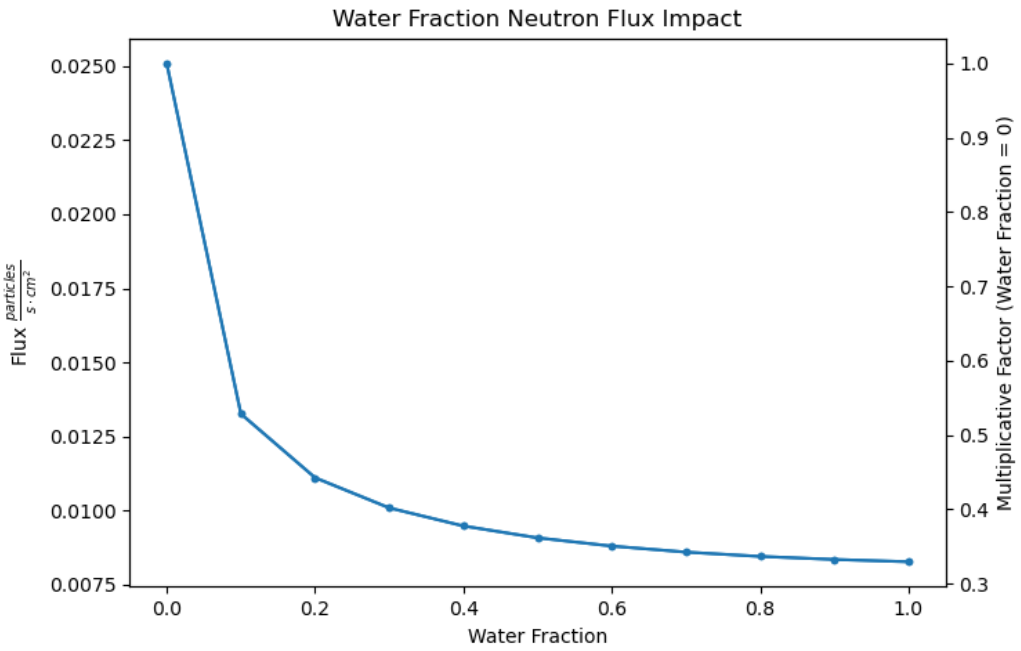

FIG. 10. Neutron flux at NYC changing with water fraction in the ground. As the water fraction increases in the ground the neutron flux decreases. Plot created using data from EXPACS.

measured.

The neutron flux can be reduced with an increase of the water fraction. This trend is shown in Figure 10. As the water fraction increases, the neutrons can interact with the water molecules and lose energy in these interactions. The neutron flux spectrum came from EXPACS using the same inputs for the Gordon Spectrum. The neutron flux was calculated by integrating the neutron spectrum over 0.01 eV – 897 GeV and the resulting values were plotted. The water fraction was changed in increments of 0.1 from 0 to 1.

C. Calculated Tritium Production Rates

Two production rate calculations were made to understand the impact of location and travel history on tritium buildup within silicon. The first calculation was made in New York City, United States and the second followed a flight from Paris, France to New York City, United States.

The neutron flux, neutron-induced tritium production in silicon cross section, and number density were integrated, using Simpson's Rule, over 11 MeV – 5 GeV (same as silicon cross section energy range) using 1 thousand evenly space intervals. For each test point within the interval, the energy value can easily be plugged into the Gordon Analytical Fit to create the neutron flux spectrum. The cross section data was interpolated using a cubic fit for evaluation of each test point. The calculated production rate is 106 atoms/kg/day. This is the same value as calculated by Saldanha et.al [9]. When using the EXPACS spectrum, this gives a production rate of 93 atoms/kg/day, a 13.1% percent difference when compared to the Gordon spectrum. This is within the experimental uncertainty of the Gordon neutron flux measurements, which are estimated to be between 10-15% above 10 MeV [14].

A similar procedure was carried out for Flight AFR10, Paris Charles de Gaulle Airport to John. F. Kennedy International Airport on a Boeing 777-300ER which lasted for 7 hours and 52 minutes. The flight data location was taken from Flight Aware which provided the time, latitude, longitude, and elevation of the aircraft along the flight path. During accent and decent, sampling was taken every 5 minutes. At cruising altitudes, sampling was increased to 15 minutes. Each location information was fed into EXPACS using the pilot-location and an aircraft mass of 1.850 100ton for operating empty weight (OEW) and 3.875 100ton for maximum takeoff weight (MTOW).

The neutron energy spectrum integration range is between 8.97 MeV to 897 GeV with 1 million evenly spaced intervals. To integrate over this energy range, a constant extrapolation at the highest energy value in the silicon cross section was used for each point after 5 GeV (last energy value in the cross section data). Each sample neutron flux spectrum and the silicon cross section data were interpolated using a cubic fit to be evaluated at each test point. Each sample neutron spectrum was multiplied by the silicon cross section, number density, integrated using Simpon's Rule, and multiplied by the sample time to result in tritium production rates for each sample. All the samples were summed up to get a tritium production rate of 11,098 (MTOW) - 12,556 (OEW) atoms/kg/trip.

III. COMPUTATIONAL TOOL

We desire to compare different travel routes to minimize the tritium buildup within the silicon to be used for detectors. We are developing a computation tool that can interpolate the neutron, photon, proton, muon-, and muon+ flux energy spectrum as a function of latitude, longitude, and altitude. The goal is to be able to obtain particle fluxes and tritium production rates that are accurate to within 10% of using exact values from EXPACS.

A. Purpose of Tool

EXPACS strength comes from the ability for the user to input any condition and receive a flux spectrum. While this output is great for analyzing single locations, the process becomes time intensive when looking at multiple locations in succession such as travel routes. We have developed a computation tool that interpolates the cosmic ray flux over the earth by creating a 3 dimensional grid that spans longitude, latitude, and altitude.

By interpolating the flux spectrum and production rate given a set of latitude, longitude, and altitude bins which their respective flux spectrums, one can reduce the time spent calculating flux spectrums and now acquire knowledge of the cosmic ray flux over any travel path. This computation tool can also calculate production rates not just for tritium

but for any nuclear process if the cross-section data for the process is inputted into the computational tool.

By inputting a file containing the travel path as a function of latitude, longitude, altitude (and time for production rate calculations), one can easily calculate a particle flux spectrum (and production rate) over any travel path.

B. Factors to Consider

As shown in Section II, the cosmic ray flux depends on latitude, longitude, altitude, surround environment, and the solar cycle which are all inputs within EXPACS. We have focused on creating bins for latitude, longitude, and altitude as our interest lies in cosmic ray flux spectrums over different paths.

In our case, we are interested in the movement of silicon for CCD development and we have used the latest date available in EXPACS: May 25, 2020. This data was chosen, as of publication of this report, as the latest quiet sun will occur in 2020-2021 [18] and the cosmic ray flux will decrease in value until 2024 (next active sun period) [19] at which the cosmic ray flux with begin to increase. The ground with a water fraction of 0.15 was chosen as the surrounding environment . These conditions were chosen to provide an upper limit on our production rate calculation as we wish to minimize the tritium buildup within silicon.

C. Development of Computational Tool

We have chosen our binning to achieve the desired 10% deviation from the true EXPACS value for a give location by binning latitude, longitude, and altitude such that there is less that 10% difference between each bin's cosmic ray flux for neutrons. The bins for latitude and longitude were created using the data presented in Section II. There are 27 latitude bins and 28 longitude bins. Figure 11 shows the Relative Intensity Factor (a multiple of cosmic ray flux at sea level) using the EXPACS inputs for Figure altitude. Nuclear interactions are of interest and the integrated energy range is 11.3 MeV – 897 GeV. Each of the particle's energy spectrum was integrated over this energy range and plotted as a function of altitude. With EXPACS being developed for altitudes, lower than 20km, we have decided to ignore altitudes higher than 20km with the highest realistic altitude would be cruising altitude of a commercial airplane which ranges about 10km to 15km. This is below the recommended 20km altitude and justifies ignoring bins higher than 20km. This results in 76 bins for altitude and final number of 57,456 grid sections for our computational tool to interpolate over. A copy of our binning is shown in Appendix A, Table II.

Our computational tool was developed using the following Python packages for the production rate interpolation: Pandas (reading data files), Numpy (data manipulation), and Scipy (data interpolation). The neutron flux spectrum is evaluated at each point in our predetermined bins and stored as a CSV file. A variable is assigned for the binning data file (CSV), one for the particle flux energy spectrum, one for the path file, and another for the nuclear cross section of interest (we used the silicon cross section).

From the variable containing the binning points, new variables are created for the latitude, longitude, and altitude respectively as numpy arrays. These three variables be used to create a multidimensional grid.

A variable is created defining the energy range to be used in the production rate calculation. Another variable is created that contains that differential flux at the binning points and will be used during the grid interpolation. Two variables are created from the path file: one variable contains the location coordinates (latitude, longitude, altitude) and the other containing the time spent at each of the location coordinates.

As done in Section II, the silicon cross section data was extended to be integrated over the desired energy range. The cross section data was interpolated using a spline interpolation to be evaluated at any energy value.

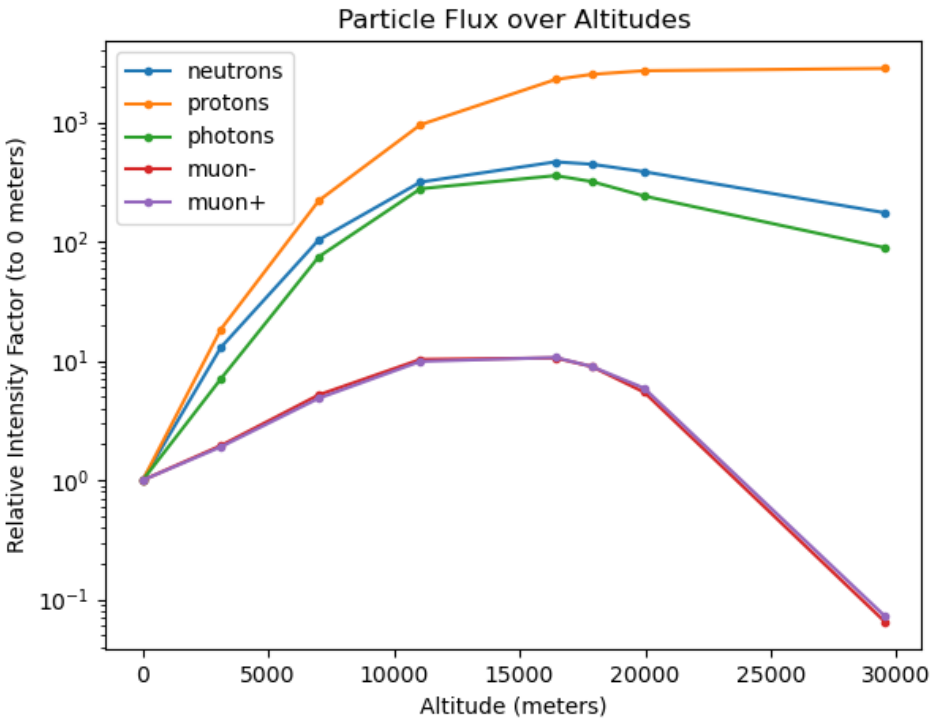

FIG. 11. Plotting the Relative Intensity of the neutron flux at different altitudes as a multiplicative factor to sea level. The integrated energy range is 11.3 MeV to 897 GeV

The production rates are calculated at each of the bin points by multiplying the differential neutron energy flux by the cross section and number density and integrated using Simpson's rule over the predetermined energy range. These values are put into a numpy array spanning latitude, longitude, and altitude (the order must match the same order as in the path file for proper interpolation). The neutron cosmic ray flux is interpolated over the multidimensional grid created with latitude, longitude, and altitude being the major axis interpolating over.

This interpolation can now be evaluated using with the variable containing the path coordinates and multiplied by the time spent at each coordinated to get the interpolated production rate for the path of interest.

D. Project Status

The model described has been tested on single grid section to find and correct bugs in the code. The C++ version of EXPACS is being used to create the data files for the bins to be inputted into the computation tool. The next step is to create a similar program to provide a particle flux energy spectrum for neutrons, protons, photons, and muons for any given path. The particle flux energy spectrum is still be developed while the production rate interpolate code is being prepared to be tested over the predetermined bins. The next steps would be to compare the results to the calculated production rates made in Section II.

IV. DISCUSSION

By creating a functioning code that can interpolate production rates over travel paths and interpolate the cosmic ray particle flux for neutrons, protons, photons, and muons reduces the time spent analyzing individual locations along the travel path. Production rates can be calculated over paths to determine the most suitable shipping routes for materials like silicon to be used in rare event experiments such as searches for dark matter.

Further work on this computation tool can be made to include the effect of the solar cycle on cosmic ray fluxes to better understand how the cosmic ray flux changes with the solar activity for long term projects concerned with cosmogenic activation. The surrounding environments can be included into the computational tool to provide a more versatile interpolation for analysis.

While it is desirable to include more variables into the computational tool, there is a compromise between accuracy of the interpolation by including more user inputs and speed of calculation using this tool.

ACKNOWLEDGMENTS

This work would not have been possible without the support, guidance, and mentoring of Richard Saldanha. His time and dedication to make this internship and project as enriching as possible is greatly appreciated. This work was supported in part by the U.S. Department of Energy, Office of Science, Office of Development for Teachers and Scientists (WDTS) under the Science Undergraduate Laboratory Internships (SULI) program.

Appendix A: Grid Binning Locations

TABLE II. A table that contains that binning used for development of our computational tool that spans latitude, longitude, and altitude.

Latitude	Longitude	Altitude	
-180	-90	0	3720
-170	-60	67.3	3830
-160	50	150	3950
-150	-40	233	4070
-140	-35	316	4190
-130	-30	400	4310
-125	-27.5	485	4430
-120	-25	571	4550
-115	-22.5	657	4680
-110	-20	743	4800
-90	-15	831	5000
-65	-10	919	5190
-60	0	1010	5390
-56	10	1100	5600
-53	20	1190	5810
-50	25	1280	6020
-40	30	1370	6240
-30	32	1460	6460
-20	34	1550	6690
40	36	1650	6930
80	37	1740	7170
180	38	1840	7420
	39	1930	7680
	40	2030	7940
	42.5	2130	8210
	45	2230	8500
	50	2330	8790
	90	2430	9090
		2530	9510
		2630	9950
		2740	10400
		2840	11100
		2950	11700
		3050	12500
		3160	16400
		3270	17900
		3380	18800
		3490	19300
		3600	

[1]M. Lisanti, "Lectures on dark matter physics," in *New Frontiers in Fields and Strings: TASI 2015 Proceedings of the 2015 Theoretical Advanced Study Institute in Elementary Particle Physics* (World Scientific, 2017) pp. 399–446.
[2]R. Narayan and M. Bartelmann, "Lectures on gravitational lensing," (1996), arXiv:astro-ph/9606001 [astro-ph].
[3]A. Aguilar-Arevalo, D. Amidei, D. Baxter, G. Cancelo, B. Cervantes Vergara, A. Chavarria, E. Darragh-Ford, J. de Mello Neto, J. D'Olivo, J. Estrada, and et al., "Constraints on light dark matter particles interacting with electrons from damic at snolab," Physical Review Letters **123** (2019), 10.1103/physrevlett.123.181802.
[4]J. Tiffenberg, M. Sofo-Haro, A. Drlica-Wagner, R. Essig, Y. Guardincerri, S. Holland, T. Volansky, and T.-T. Yu, "Single-electron and single-photon sensitivity with a silicon skipper ccd," Physical Review Letters **119** (2017), 10.1103/physrevlett.119.131802.
[5]A. Aguilar-Arevalo, D. Amidei, X. Bertou, D. Bole, M. Butner, G. Cancelo, A. C. Vázquez, A. Chavarria, J. d. M. Neto, S. Dixon, and et al., "Measurement of radioactive contamination in the high-resistivity silicon ccds of the damic experiment," Journal of Instrumentation **10**, P08014–P08014 (2015).
[6]J. F. Ziegler, "Terrestrial cosmic rays," IBM Journal of Research and Development **40**, 19–39 (1996).
[7]S. Cebrián, "Cosmogenic activation of materials," International Journal of Modern Physics A **32**, 1743006 (2017), https://doi.org/10.1142/S0217751X17430060.
[8]T. B. C.Dunford, "Online nuclear data service," (1998).
[9]R. Saldanha, R. Thomas, R. H. M. Tsang, A. E. Chavarria, R. Bunker, J. Burnett, S. R. Elliott, A. Matalon, P. Mitra, A. Piers, P. Privitera, K. Ramanathan, and R. Smida, "Cosmogenic activation of silicon," (2020), arXiv:2007.10584 [physics.ins-det].
[10]T. Sato and K. Niita, "Analytical Functions to Predict Cosmic-Ray Neutron Spectra in the Atmosphere," Radiation Research **166**, 544–555 (2006), https://meridian.allenpress.com/radiation-research/article-pdf/166/3/544/2140600/rr0610_1.pdf.
[11]T. Sato, H. Yasuda, K. Niita, A. Endo, and L. Sihver, "Development of PARMA: PHITS-based Analytical Radiation Model in the Atmosphere," Radiation Research **170**, 244–259 (2008), https://meridian.allenpress.com/radiation-research/article-pdf/170/2/244/2155866/rr1094_1.pdf.
[12]T. Sato, "Analytical model for estimating terrestrial cosmic ray fluxes nearly anytime and anywhere in the world: Extension of parma/expacs," PLOS ONE **10**, 1–33 (2015).
[13]T. Sato, "Analytical model for estimating the zenith angle dependence of terrestrial cosmic ray fluxes," PLOS ONE **11**, 1–22 (2016).
[14]M. S. Gordon, P. Goldhagen, K. P. Rodbell, T. H. Zabel, H. H. K. Tang, J. M. Clem, and P. Bailey, "Measurement of the flux and energy spectrum of cosmic-ray induced neutrons on the ground," IEEE Transactions on Nuclear Science **51**, 3427–3434 (2004).
[15]W. N. Hess, H. W. Patterson, R. Wallace, and E. L. Chupp, "Cosmic-ray neutron energy spectrum," Phys. Rev. **116**, 445–457 (1959).
[16]E. Hughes and P. Marsden, "Response of a standard igy neutron monitor," Journal of Geophysical Research **71**, 1435–1444 (1966).
[17]J. Nevalainen, I. Usoskin, and A. Mishev, "Eccentric dipole approximation of the geomagnetic field: Application to cosmic ray computations," Advances in Space Research **52**, 22 – 29 (2013).
[18]S. K. Bisoi, P. Janardhan, and S. Ananthakrishnan, "Another mini solar maximum in the offing: A prediction for the amplitude of solar cycle 25," Journal of Geophysical Research: Space Physics **125**, e2019JA027508 (2020), e2019JA027508 10.1029/2019JA027508, https://agupubs.onlinelibrary.wiley.com/doi/pdf/10.1029/2019JA027508.
[19]P. Bhowmik and D. Nandy, "Prediction of the strength and timing of sunspot cycle 25 reveal decadal-scale space environmental conditions," Nature Communications **9**, 1–10 (2018).

Pacific Northwest National Laboratory

902 Battelle Boulevard
P.O. Box 999
Richland, WA 99354

1-888-375-PNNL (7665)

www.pnnl.gov